

Observations of banding in first-year Arctic sea ice

David M. Cole

U.S. Army Cold Regions Research and Engineering Laboratory, Hanover, New Hampshire, USA

Hajo Eicken, Karoline Frey,¹ and Lewis H. Shapiro

Geophysical Institute, University of Alaska–Fairbanks, Fairbanks, Alaska, USA

Received 2 June 2003; revised 5 March 2004; accepted 10 May 2004; published 14 August 2004.

[1] Horizontal banding features, alternating dark and bright horizontal bands apparent in ice cores and stratigraphic cross sections have long been observed in first-year sea ice and are frequently associated with bands of high and low brine or gas porosity. Observations on the land-fast ice near Barrow, Alaska, in recent years have revealed particularly striking banding patterns and prompted a study of their macroscopic and microscopic characteristics. The banding patterns are quantified from photographs of full-depth sections of the ice, and examples are presented from the Chukchi Sea and Elson Lagoon. Statistics on band spacing are presented, and the growth records for three seasons are employed to estimate their time of formation. These data provide insight into the periodicity of the underlying phenomena. Micrographs are used to examine the microstructural variations associated with various banding features and to quantify the geometry of the constituent brine inclusions associated with high- and low-porosity bands. The micrography revealed that the area fraction of brine inclusions varied by a factor of nearly 3 through the more pronounced high- and low-porosity bands. Vertical micrographs obtained shortly after the materials' removal from the ice sheet showed that significantly larger inclusions form abruptly at the start of the high-porosity bands and frequently terminate abruptly at the end of the band.

Crystallographic observations indicated that the high-porosity bands supported the nucleation and growth of crystals having substantially different orientations from the very well aligned columnar structure that characterized the bulk of the sheet. *INDEX TERMS:* 4540

Oceanography: Physical: Ice mechanics and air/sea/ice exchange processes; 4524 Oceanography: Physical: Fine structure and microstructure; 4599 Oceanography: Physical: General or miscellaneous; 4215 Oceanography:

General: Climate and interannual variability (3309); *KEYWORDS:* banding, Arctic, sea ice

Citation: Cole, D. M., H. Eicken, K. Frey, and L. H. Shapiro (2004), Observations of banding in first-year Arctic sea ice, *J. Geophys. Res.*, 109, C08012, doi:10.1029/2003JC001993.

1. Introduction

[2] First-year sea ice typically exhibits horizontal banding features to varying degrees [e.g., *Bennington*, 1963b]. Certain banding features associated with microstructural gas and brine porosity variations appear in thin ice as a consequence of the conditions during freeze-up and freezing rate variations, and banding at depth is associated primarily with brine porosity variations. On a fundamental level, the study of banding features provides an opportunity to gain insight into the relationships between the conditions during freezing (i.e., thermal history, under-ice currents) and the resulting ice properties. Additionally, these features are of interest because the associated inclusions dominate the optical [*Perovich and Gow*, 1996; *Perovich et al.*, 1998], electromagnetic [*Perovich and Gow*, 1991], thermal [*Schwerdtfeger*, 1963; *Niedrauer*

and *Martin*, 1979], and mechanical [*Cole et al.*, 1995; *Cole and Durrell*, 2001] properties of sea ice. The present effort was prompted both by this broad base of interest and by observations of noticeable differences in the number and prominence of banding features in recent years compared with previous (1993–1994) years. The intent of the present paper is to document the occurrence of bands through several seasons at specific locations and to describe the underlying porosity and microstructural variations associated with these features. Such information is fundamental to developing a comprehensive understanding of sea ice growth processes and supports a quantitative analysis that will be presented in a subsequent paper.

[3] The work was part of a multiyear effort to explore the development and evolution of the physical properties, thermodynamics, and permeability of first-year sea ice in the Alaskan Arctic [*Cole and Shapiro*, 1998; *Eicken et al.*, 2000; *Frey et al.*, 2001; *Perovich et al.*, 2001]. In support of this program, monitoring sites were established in the Chukchi Sea and in nearby Elson Lagoon to record the thermal history, growth rate, and physical properties profiles

¹Deceased 24 March 2002.

of land-fast, first-year sea ice. An extensive suite of observations of the flaw structure, on scales ranging from the full thickness of the sheet to that of individual brine inclusions, was made on first-year ice very soon after its removal from the sheet. Recognizing that any particular method of observation has advantages and drawbacks, the overall effort employed a variety of sampling, photographic, and imaging techniques [Cole and Shapiro, 1998; Eicken et al., 2000]. However, the work presented below employs standard photographic methods for full-depth sections and uses photomicrography to acquire images from sets of orthogonal thin sections. These images document the complex brine inclusion structure and support a quantitative analysis of the variations in pore microstructure associated with the horizontal bands. The present effort examines a variety of banding features and presents a detailed examination of a number of high- and low-porosity bands in order to elucidate their fundamental physical nature and gain insight into the processes that lead to their formation. A subsequent publication will examine potential mechanisms for the formation of the observed bands.

2. Previous Observations of Banding in Sea Ice

[4] Bennington [1963a, 1963b, 1967] has contributed substantially to studies of the development and evolution of the physical properties of sea ice, both with laboratory and field observations of banding and brine drainage features. Ignoring features associated with deformation, Bennington [1963b, 1967] identified three types of banding features: those associated with a c-axis vertical microstructure, those associated with high porosity zones, and those associated with the expansion of trapped brine pockets as a result of warming during ice evolution (sometimes referred to as brine corrosion).

[5] Bennington [1963a] examined banding in first-year sea ice and presented a chemical analysis to address the issue of fractionation of Cl^- , Na^+ , SO_4^{2-} , Mg^{2+} , Ca^{2+} , and K^+ during the freezing of sea ice. Particular attention was paid to determining whether the bulk concentration of these ions varied with the observable banding features. The analysis indicated that the relative concentrations of the ions in the sea ice were essentially the same as in the seawater and apparently did not vary with the banding features.

[6] Significantly, banding is not a land-fast ice or near-shore phenomenon, as demonstrated by repeated observations of banding features of comparable spacing and width during the 2002 spring Shelf-Basin Interactions (SBI) cruise in the Chukchi and Beaufort Sea. Gow et al. [1987a] found banding in many of the floes that were examined in Fram Strait during MIZEX-84. Nor is banding restricted to the Arctic: Gow et al. [1987b] observed banding in congelation ice in the Weddell Sea pack ice, with the number of bands varying up to 30 m^{-1} . Furthermore, horizontal banding features have been observed in first-year sea ice in McMurdo Sound, Antarctica, in the vicinity of the Dellbridge Islands [Smith et al., 1998; Verbeke et al., 2002], and near Cape Barne in October 2000 and November 2001 under another program ("Field studies and modeling of the breakup of Antarctic sea ice," OPP 9909100). Verbeke et al. [2002] analyzed the periodicity of horizontal banding ob-

served in first-year sea ice in McMurdo Sound, Antarctica. That work assessed potential mechanisms of band formation such as thermal fluctuations and under-ice current variations, and concluded that the bands were related to tidal fluctuations that brought about variations in the under-ice salt concentration.

[7] Adams et al. [1963] presented laboratory data that showed a tendency for the salinity of forming ice to decrease as the under-ice current velocity increased. This relationship has been studied in greater detail more recently in the laboratory: observations of Eicken et al. [2000] show that growth in the presence of an under-ice current produces a substantial reduction in brine volume relative to growth under quiescent conditions. The above findings thus establish a reasonable expectation that variations in under-ice conditions can give rise to substantial salinity variations in a growing ice sheet.

3. Methods and Observations

[8] Although some bands are closely linked with changes in the size and orientation of the constituent ice grains, crystallographic variations per se do not produce visibly evident bands. Rather, the optical effect arises because of the interaction of light either with brine inclusions or bubbles. Because of the greater contrast in refractive indices and impact on light scattering, gas-filled inclusions (either drained brine inclusions or bubbles) generally constitute the most visually evident bands [see Light et al., 2003]. However, some banding is associated with abrupt changes in crystallography: fine-grained frazil ice can produce a band with a high concentration of both brine- and gas-filled inclusions, and bands of small, c-axis-vertical crystals have characteristic brine inclusions that are oriented horizontally [Bennington, 1967]. Nonetheless, very pronounced bands can occur in uninterrupted columnar ice. Bands associated with gas-filled inclusions are immediately evident upon removal of a specimen from an ice sheet. Bands associated with a population of interconnected brine-filled inclusions become clearly visible only after some brine drainage has occurred. The Arctic sea ice sheets examined in the present effort typically contain one or two bands of fine-grained ice in the top 0.2 m, and the banding features at lower depths are associated with variations in the distribution of brine-filled inclusions in a columnar microstructure. For the sake of completeness, subsequent sections describe bands caused by variations in crystallography, gas porosity, and brine porosity, although attention is focused primarily on bands associated with variations in brine porosity.

[9] We extracted full-depth sections measuring $\sim 0.6 \text{ m}$ long and $\sim 40 \text{ mm}$ thick at the monitoring sites indicated in Figure 1. The vertical dimension was the thickness of the ice sheet. The coordinates of the Chukchi Sea site are $71^\circ 19.64' \text{N}$ $156^\circ 42.13' \text{W}$, and those of the Elson Lagoon site are $71^\circ 21.13' \text{N}$ $156^\circ 31.26' \text{W}$.

[10] As previously demonstrated, ice formed at the field sites in the Chukchi Sea and Elson Lagoon typically develops a strong preferred c-axis orientation after a relatively short (e.g., 0.3 m) amount of growth [Weeks and Gow, 1978; Cole and Shapiro, 1998]. To investigate the potential relationship between crystal alignment and the banding and brine drainage features, we obtained orthogonal sets of full-

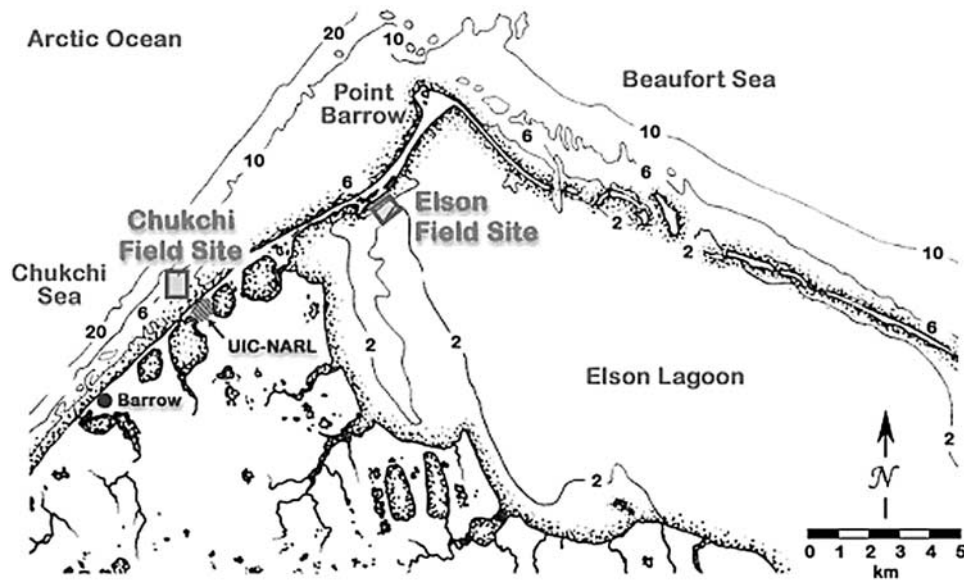


Figure 1. Location of instrumentation sites in the Chukchi Sea and Elson Lagoon (water depths are given in meters).

depth sections as well as thin sections, with their viewing direction oriented either perpendicular (\perp) or parallel (\parallel) to the preferred c-axis direction.

[11] The extent to which the banding features are evident to the unaided eye is a function of the ice section thickness in the viewing direction and its overall age. All but the most pronounced bands are not readily evident if the thickness of the section is less than the characteristic spacing of the constituent brine inclusions (or clusters of inclusions). For this reason, it is difficult to capture such features in vertical thin sections. On the other hand, light scattering even in the low-porosity bands makes it difficult to distinguish bands in sections that are too thick. Thickness in the range of 20–40 mm generally produces optimal viewing. Sample age, temperature, and exposure are also considerations. Typically, high-porosity bands will become evident after several minutes of brine drainage and remain relatively distinct for some time, depending on the environmental conditions. Continued drainage, exposure to sunlight, and increasing surface roughness due to sublimation eventually degrade their appearance.

[12] Figures 2a–2l show 12 examples of the full-depth sections obtained on the indicated dates over a period of several years. The sections were obtained from approximately the same location in the Chukchi Sea in the spring of the years 1995 and 1999–2002, and for 1994 and 2001–2002 at the Elson Lagoon site. The observations of 1994 and 1995 were made under a previous field program as described by *Cole and Shapiro* [1998]. Note that the horizontal bands are occasionally disrupted by the vertical drainage features, but generally persist throughout the sheet. In addition to the high-porosity bands in the upper 0.1 to 0.2 m of the sheets (which are usually associated with bands of fine-grained granular ice), alternating light and dark bands are evident throughout the bulk of most of the full-depth sections. However, the years 1995 at the Chukchi Sea site and 1994 and 2002 at the Elson Lagoon site have

notably fewer banding features than the other years. Figure 2a shows an overplot of $\delta^{18}\text{O}$ (stable-isotope data have been measured at the Stable-Isotope Laboratory at the Arctic Research Center, University of Alaska, Fairbanks) and salinity as a function of depth, and Figures 2c and 2k show overplots of the salinity only. The profile in Figure 2c shows salinities obtained for depth ranges that corresponded approximately to visually evident changes in structure or porosity. Approximately 2 months before the full depth section shown in Figure 2k was obtained, the profile in Figure 2k shows salinities that were measured in the field at 0.01-m intervals. At that point, the sheet was 0.85 m thick, so the salinity profile does not extend to the bottom of the full-depth section photograph. Ignoring the expected increase in salinity near the bottom of the profile, the plot shows a correspondence between the location of the bright bands and local peaks in the salinity profile. It is evident that resolution on the scale of 0.01 m or less is required to capture the salinity variations associated with these banding features.

[13] Comparison between the banding features at the two study sites was hampered by the fact that storms in the fall of 1998 and 1999 formed zones of sediment-rich frazil ice through more than the upper 0.5 m of the ice sheet in Elson Lagoon [*Stierle and Eicken*, 2002]. As a result, the ice was rendered useless for the purposes of this study, so full-depth sections were obtained in Elson Lagoon only for the winters of 2000–2001 and 2001–2002.

[14] Occasionally, relatively thin bands (e.g., <10 mm) occur that appear to be exceptionally clear to the unaided eye. As demonstrated below, these bands are devoid of all but the smallest brine inclusions. In addition, in Elson Lagoon we have on occasion observed bands of exceptionally high gas porosity relatively deep in the sheet (~ 0.8 m). A particularly porous band, consisting of very large (10–20 mm diameter) gas bubbles, appeared in the 2000–2001 season. Figure 3 shows a photograph of material from this

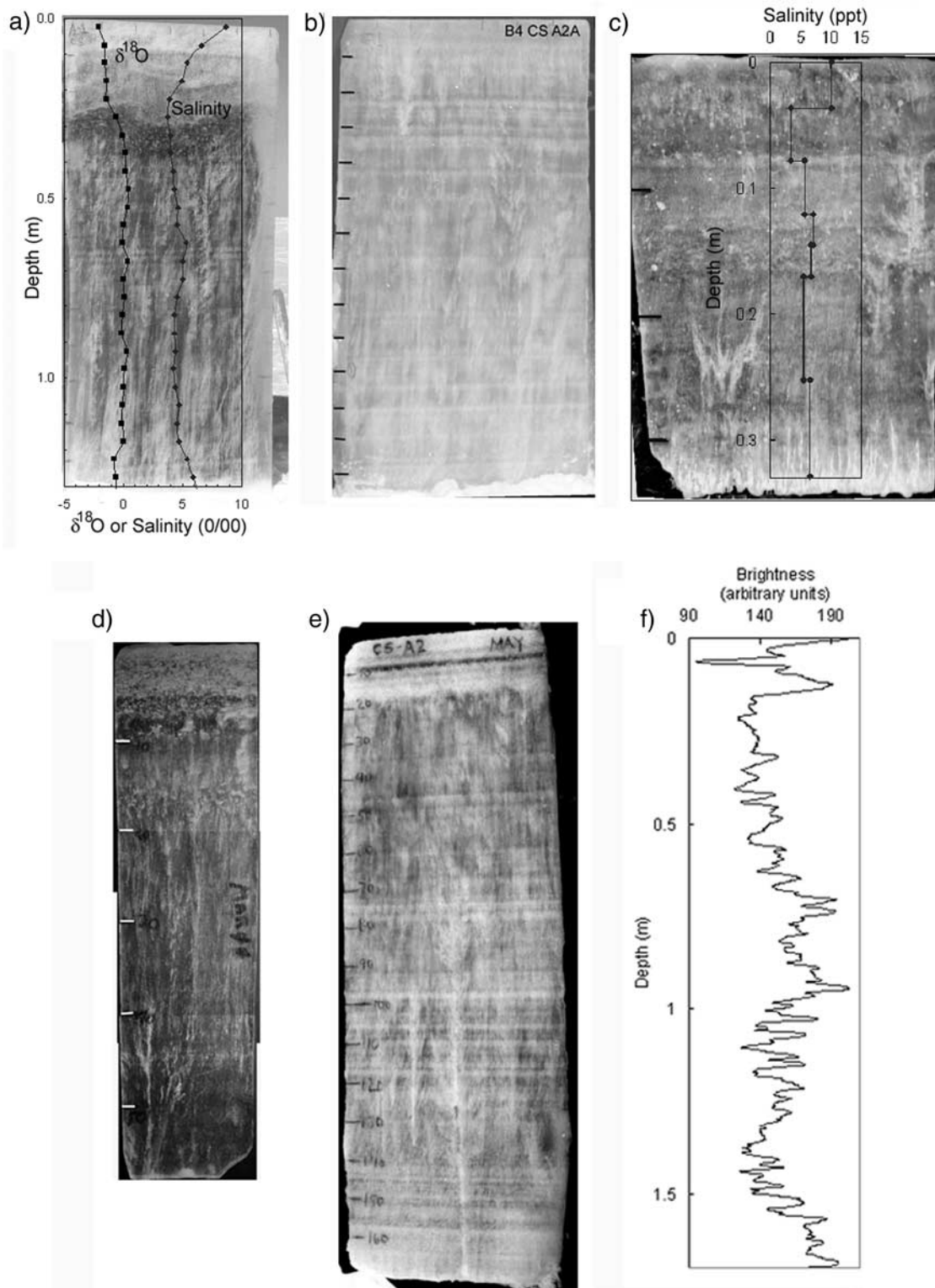


Figure 2. Full-depth section photographs. Chukchi Sea site: (a) May 1995 (\perp), (b) May 2000 with the preferred c-axis direction running in-plane (\perp), (c) May 1999 with the salinity profile superimposed, (d) March 2000 (\perp), (e) May 2000, (f) the average brightness profile for the section shown in Figure 2e (\perp), (g) April 2001 showing a large array of diagonal brine tubes (\parallel), (h) May 2001 (\perp), and (i) May 2002 (\parallel). Elson Lagoon site: (j) March 1994, (k) April 2001 (\perp), and (l) May 2002 (\perp). Index marks are spaced at 0.10 m in all cases. The symbols \parallel and \perp in the captions indicate, respectively, that the viewing direction is parallel or perpendicular to the preferred c-axis direction.

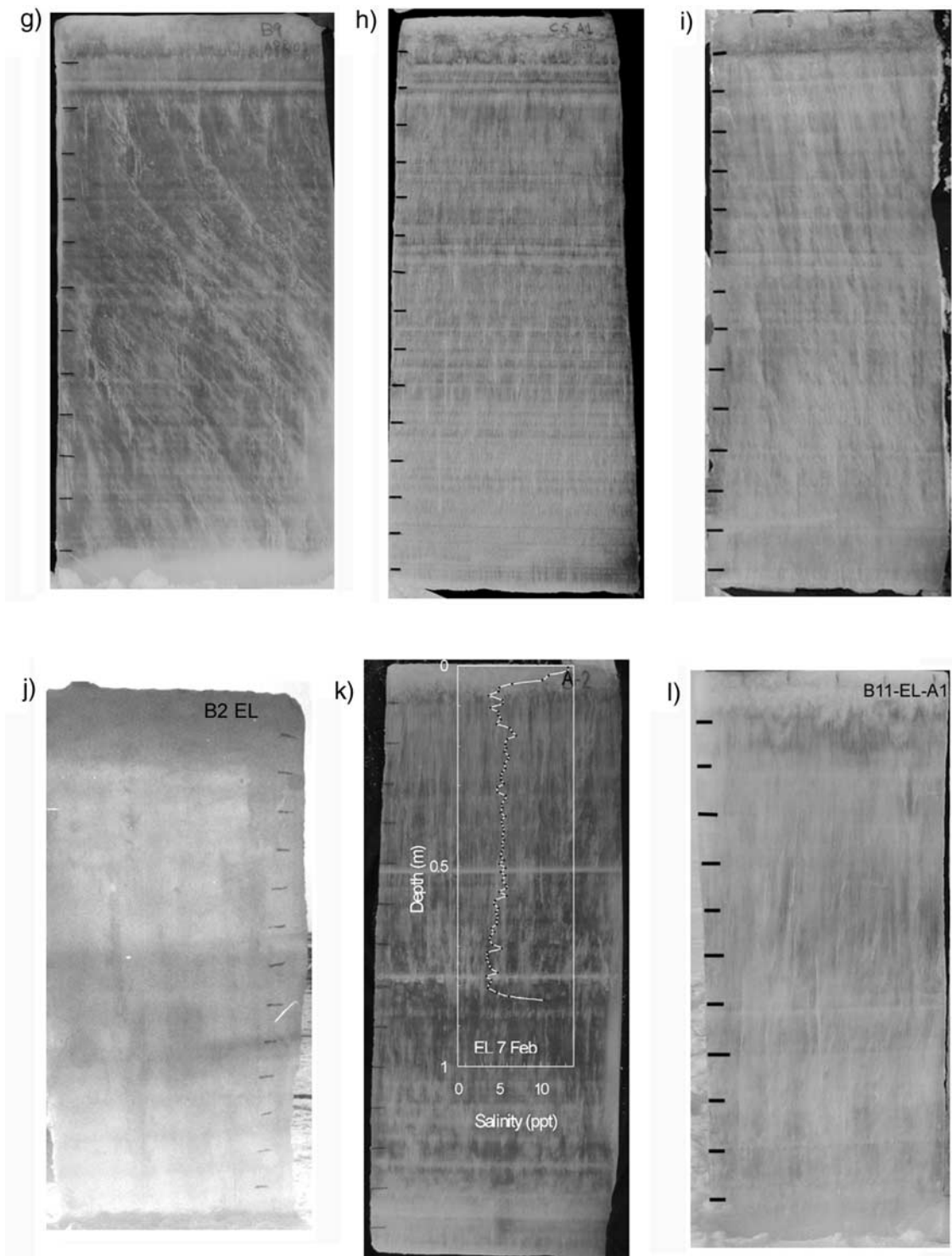


Figure 2. (continued)

band. The voids have been filled with ice shavings to provide contrast. From their shape, it is evident that these voids are gas bubbles that were presumably released from the floor of the lagoon and were subsequently incorporated into the growing ice sheet. Because of their depth (0.8 m), and the fact that the study site was >6 km from the ice edge when this band formed, it is extremely unlikely that the gas

bubbles would have originated from air entrained in the water column by turbulence. The highly porous band introduces a plane of weakness and constitutes a significant optical and thermal barrier in the center of the sheet. Although we were not equipped to analyze the gas in these inclusions, we presume that it originated from the floor of the lagoon, which is 2.2 m deep at the test site. *Phelps et al.*

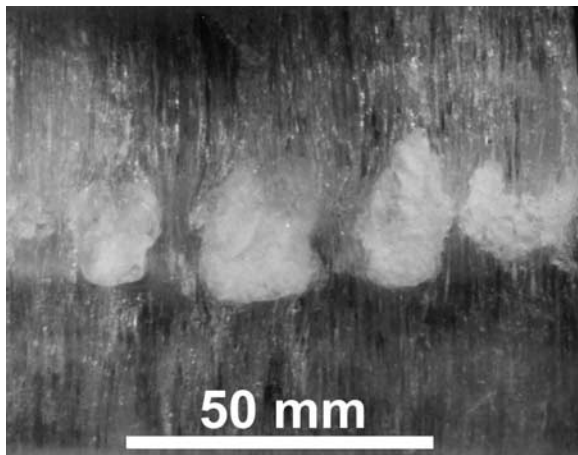


Figure 3. Photograph of a high gas porosity band found in Elson Lagoon, April 2001 (see band in Figure 2k at a depth of approximately 0.80 m). The large bubbles have been filled with ice shavings to provide some contrast with the surrounding material.

[1998] and *Phelps and Jeffries* [1999] found methane in a study of the composition of the gas found in lake ice bubbles in the Barrow area, so a mid-winter methane release is not unrealistic for this area. No corresponding band was found at the Chukchi Sea site, and although this band extended over the Elson Lagoon study area, its actual lateral extent is not known. Interestingly, *Cole and Shapiro* [1998] found a similar, but much less porous band of bubbles in Elson Lagoon.

4. Microscopic Observations

[15] A nearby facility (UIC-NARL, see Figure 1) provided cold room space for conducting the microstructural analysis and obtaining optical micrographs (see *Cole and Shapiro* [1998] for a detailed description of the equipment and procedures). In addition to horizontal thin sections obtained at 0.1-m intervals from cores drilled adjacent to the full-depth sections, two orthogonal vertical thin sections were obtained at each depth interval. As noted in the preceding section, the ice at the Chukchi Sea site showed a very strong c-axis alignment in the horizontal plane in a direction parallel to the shoreline. Consequently, the viewing directions of the vertical sections were taken parallel and perpendicular to the preferred c-axis direction. In addition, we obtained horizontal sections in the center of several representative high- and low-porosity bands (a total of six bands were characterized) to support a quantitative analysis of the inclusion geometry. Most of the images of the horizontal sections were taken with nonpolarized transmitted light, and we obtained polarized images in representative cases to show the location of the inclusions with respect to crystallographic features.

[16] The micrography system used conventional 35-mm film, and the resulting images were scanned with a resolution of 300 dpi. For the magnifications of 6.5X to 16X that were employed for these observations, a pixel in the digitized image corresponded to a physical dimension of between approximately 8 and 3 μm , respectively. The image

processing (which employed Image Pro Plus) was conducted in a supervised mode, whereby the operator makes a visual assessment of how well the objects of interest have been identified and outlined by the program. The program identifies objects of interest within a selected area and calculates the area, aspect ratio, orientation of the object's major axis, and fraction of the total area of each object, as well as the total number of objects. Since the brine tubes are not necessarily parallel to the viewing direction, the perimeter can be somewhat difficult to define. A conservative estimate of the error in the inclusion area associated with this effect is placed at 10%.

[17] Figure 4 illustrates the inclusions as determined by the image processor. Since the larger brine inclusions that populate the high-porosity bands are typically elongated in the vertical direction, brine drains from them during preparation of the thin section. As a consequence, they appear as dark objects on a bright field. Figure 4 illustrates the good fidelity between the objects identified by the software, which appear on the right side of the figure, and the micrograph, which appears on the left side of the figure. The larger brine tubes are typically elongated in the vertical direction, so their diameters are best captured in horizontal thin sections. Vertical thin sections, on the other hand, are useful for viewing the small-scale inclusions (measuring 0.1 mm or less in diameter) that congregate along plate boundaries and are difficult to discriminate when viewed in the growth direction. Figure 5 shows examples of orthogonal views of the types of inclusions under discussion.

[18] Small, isolated, brine-filled inclusions appear as much lower contrast objects than drained inclusions (e.g., see Figure 5a) and are frequently difficult for the image analysis software to identify reliably. Additionally, it was generally necessary to increase the contrast of the images to improve the software's ability to capture the objects of interest, and this would eliminate some of the very small, low contrast inclusions. Nonetheless, the program systematically identified inclusions with minimum dimensions in

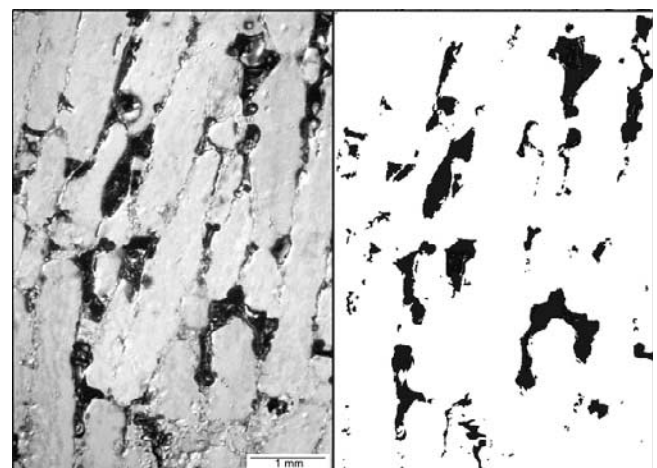


Figure 4. (left) Typical micrograph from (right) a horizontal thin section showing the outlines of the inclusions identified by the image processor. The dark objects are drained brine tubes, viewed in the direction of freezing. Micrograph is from a depth of 1.26 m in the Chukchi Sea ice sheet, April 2001.

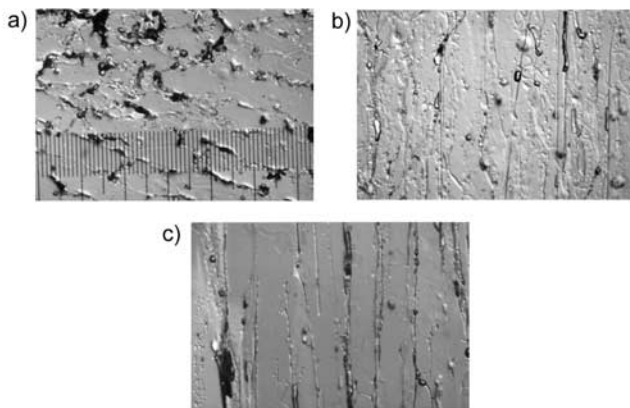


Figure 5. Micrographs showing orthogonal views of the inclusion structure at the sub-grain scale (Chukchi Sea, depth = 1.1 m, April 2000). (a) Horizontal section, viewed in the direction of freezing. (b) Vertical section, viewed parallel to the c-axis direction. (c) Vertical section of a relatively porous section of the ice, viewed perpendicular to the c-axis direction. The fine scale divisions in Figure 5a are 0.1 mm, and the other two micrographs have the same magnification. See color version of this figure in the HTML.

the range of 20–30 μm , which corresponds to inclusion areas in the 10^{-4} mm^2 order of magnitude.

[19] An examination of the orthogonal vertical sections indicates that horizontal bands typically have the same appearance in both views. However, the larger-scale inclusions (with diameters approximately equal to the plate spacing) and brine drainage features can exhibit a considerable degree of anisotropy, particularly in the case of the large diagonal arrays as seen in Figure 2g. *Cole et al.* [2002] examined these diagonal features and found that they are composed of relatively large brine inclusions having an average area of 1.2 ± 2.7 mm^2 , and their average aspect ratio is 2.8 ± 1.3 when observed in the horizontal plane. The dense network of inclusions in the view shown in Figure 2g is actually confined to a fairly narrow vertical plane that is several millimeters thick. The orthogonal view [see *Cole et al.*, 2002, Figure 5] reveals that these vertical planes are typically spaced several centimeters apart, thus giving rise to a strong anisotropy.

5. Crystallographic Observations

[20] Figure 6 shows horizontal and vertical thin sections that illustrate the crystallographic features of the banded regions. Note the well-defined frazil layer (Figure 6a) at the top of the ice sheet. A columnar structure persisted through all of the subsequent bands (Figure 6b). As observed in the past [*Cole and Shapiro*, 1998], the columnar ice matrix at the test site is typically well aligned (e.g., the sheet consists of ice grains with their c-axes in the horizontal plane and aligned in the direction of the under-ice current) and contains a significant number of small, nonpropagating grains imbedded within it. It is unclear whether these grains were simply nucleated within the growing ice matrix or were nucleated in the water column and subsequently incorporated in the sheet. However, it is noted that the latter

process is akin to the platelet ice crystals found in McMurdo Sound sea ice [see, e.g., *Cole and Dempsey*, 2004], which appear to be randomly distributed in the columnar ice matrix, rather than being confined to a very well defined band.

[21] Interestingly, although the columnar grain structure persists macroscopically throughout the bands, new grains were nucleated at the upper boundary of some high-porosity bands (see Figure 6c) but generally did not propagate beyond the high-porosity band in which they formed. Although the microscopy system was not equipped to measure the crystallographic orientation of these grains, the fact that they are distinguishable from the aligned columnar ice matrix indicates that their c-axis orientations are different from the matrix. This, in turn, indicates a loss of the preferred c-axis alignment in the horizontal plane when the small grains appear. Since it is well known that a persistent under-ice current is required to produce c-axis alignment [see *Weeks and Ackley*, 1982], it may be inferred that the loss in alignment is associated with a drop in the velocity of the under-ice current. Conversely, an increase in the velocity of the under-ice current would hamper the growth of grains that are unaligned with the prevailing current and explain their termination at the bottom of the high-porosity band.

6. Brine Inclusion Characteristics

[22] The following three sections present details of the brine inclusions found in the upper frazil band and in selected high- and low-porosity bands at depth in first-year sea ice from the Chukchi Sea in early April 2001. The terms high and low porosity in the present context are relative and not intended to suggest that the ice properties alternate between two states. As seen in the physical properties profiles, in the inclusion statistics, and in the micrographs, there can be a good deal of variation in the characteristics of what might be considered a nominally high- or low-porosity band. With regard to potential errors in the inclusions statistics presented in the following sections, it is noted that because the sections are of finite thickness, the measurement method will generally overestimate the inclusion area, except when the sides of the inclusions are aligned in the viewing direction. This error is believed to be minimal because the sections were thin (e.g., typically 1 to 2 mm), and the brine inclusions were generally well aligned in the vertical direction (as seen in Figure 5c). Finally, we use area fraction of brine pores (e.g., the sum of the areas of the brine inclusions divided by the total area evaluated) to compare the brine porosities of the bands being examined. Stereologically, the area fraction and the brine volume fraction of pores are equivalent for a representative section through the medium (Delesse theorem).

6.1. Granular Ice Band

[23] Since the banding features in the upper portion of the sheet result from microstructural and growth rate variations, their inclusion structure can be significantly different from the bands that occur at depth. A subsequent publication uses the local temperature records to estimate ice growth rates and finds a correlation between growth rate and ice prop-

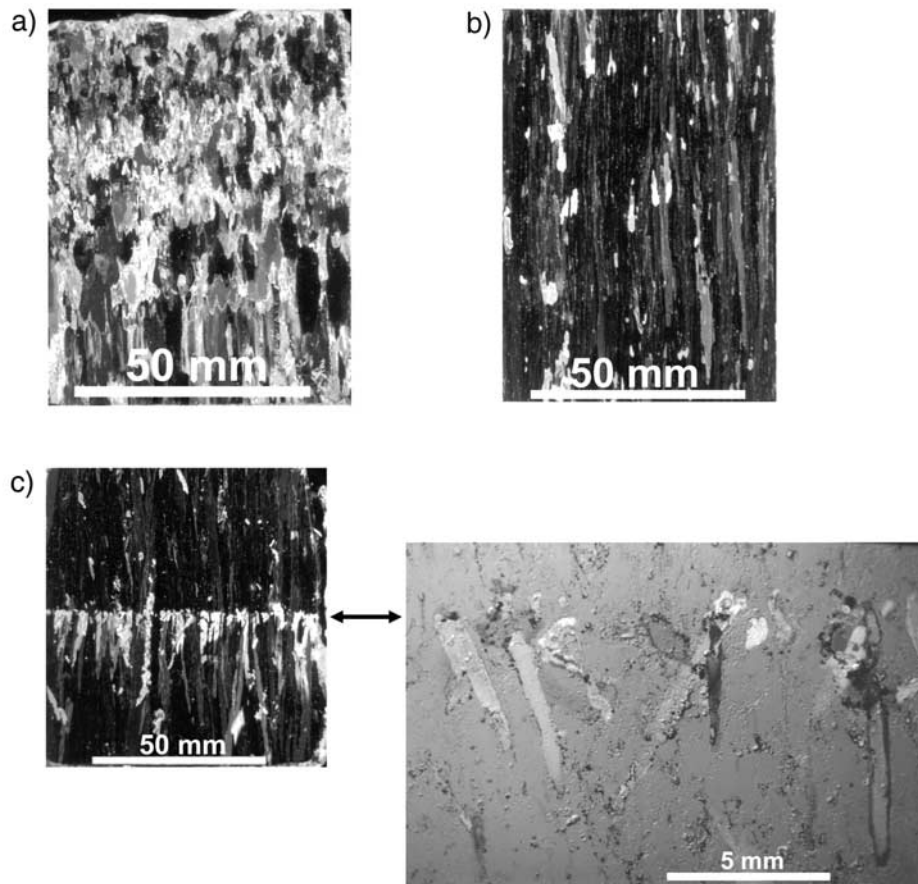


Figure 6. Photographs of vertical thin sections illustrating the crystallography associated with two types of banding features of the ice sheet. (Chukchi Sea, May 2001). (a) The fine-grained band of ice at the top of the sheet. (b) Typical columnar structure that generally persisted through the bulk of the sheet, and is typical of lower porosity bands. Note the presence of small, nonpropagating grains throughout the section. (c) Example of grain nucleation at the start of a high-porosity band as seen under cross-polarized light. These grains typically grew for only a short distance. Thin section photograph appears on the left and a 6.5X micrograph appears on the right. See color version of this figure in the HTML.

erties in the upper 0.3 m of the sheet. Figure 7 shows a composite vertical micrograph taken with unpolarized light to illustrate the nature of the inclusions in the frazil band. Such material typically contains a significant population of gas-filled inclusions (bubbles) and does not necessarily have the cellular substructure of congelation ice; the inclusions are generally arranged more randomly than farther down in the sheet. The inclusions that formed as gas-filled bubbles are generally distinguishable from drained brine inclusions because they are larger and have the shape of an oblate spheroid. Although the grains in such bands are typically randomly oriented, we have occasionally observed a band of c-axis-vertical crystals, as reported by *Bennington* [1963b].

6.2. Low-Porosity Bands at Depth

[24] Figure 8 shows a typical horizontal micrograph of a low-porosity band for the indicated time and location. Because the frame size was frequently too small to capture a representative area, the image analysis was typically conducted on 4–6 adjacent micrographs from a given thin

section. The low-porosity bands have the common characteristic of a virtual absence of brine inclusions with widths approaching the plate spacing and a preponderance of very small brine inclusions. In the horizontal plane, the average area fraction of inclusions for the low-porosity bands was 0.034 ± 0.005 . This corresponds to a salinity of 4.0‰ at an in situ temperature of -5.9°C at the time of sampling, based on *Cox and Weeks*' [1983] brine volume-salinity relations. This salinity value is lower than the bulk salinities of between 5 and 6‰ measured in a parallel core at the same depth interval. (Note that although the photographs in Figures 2a–2l indicate that the larger-scale brine drainage features frequently penetrate the low-porosity bands, the influence of those features on the inclusion statistics is not considered in the present treatment.) The largest inclusions that form in the low-porosity bands tend to have rather high aspect ratios in the horizontal plane and appear flattened in the plane of the plate boundary and elongated in the growth direction. An analysis of a representative low-porosity band indicated that $\sim 99\%$ of the inclusions had widths of <0.5 mm, and



Figure 7. Composite micrograph illustrating the inclusion structure of the fine-grained band at the top of the sheet, as viewed in a vertical thin section. Most of the large objects are drained brine inclusions.

these constituted $\sim 89\%$ of the horizontal area fraction of brine inclusions.

6.3. High-Porosity Bands at Depth

[25] Figure 9 presents a micrograph of a typical high-porosity band. The high-porosity bands can begin abruptly and, in addition to the population of smaller inclusions found in the low-porosity bands, contain a population of inclusions that are substantially larger in the horizontal cross-sectional area. Larger-diameter inclusions frequently begin at the top of such high-porosity bands, and continuous tubes occasionally exhibit an increase in diameter. When viewed in a horizontal cross section, the width of the larger brine inclusions appears to be limited by the plate spacing, and they are frequently elongated in the plane of the plate boundary. When viewed in a vertical section, they generally extend all or most of the way through the high-porosity band, frequently connecting with other inclusions. Figure 10 shows a log-log plot of the number of inclusions per unit

area versus inclusion area for the bands that were studied. For this plot, data from the three high-porosity bands have been grouped, as have the data from the three low-porosity bands, and the number of inclusions in each bin (of width 0.001 mm^2) have been normalized to the observed area of the micrographs from which they were obtained. Figure 10 illustrates the fact that the higher-porosity bands contain approximately the same area density of small inclusions (e.g., those with area $\leq 0.02 \text{ mm}^2$) as do the low-porosity bands. However, they also have a significantly larger population of large-diameter inclusions. In the horizontal plane, the average area fraction of inclusions for the high-porosity bands was 0.091 ± 0.006 , corresponding to a salinity of 7.5% for an in situ temperature of -4°C , as outlined above. Additionally, an analysis of a typical high-porosity band revealed that inclusions having widths $>0.5 \text{ mm}$ represented $\sim 5\%$ of the number of inclusions but contributed $\sim 47\%$ of the horizontal area fraction of brine inclusions.

[26] The full-depth section taken from the Chukchi Sea in December 1999 shows a high-porosity band at a depth of approximately 0.45 m that contrasts dramatically with the neighboring bands (Figure 11, left). The mosaic on the right

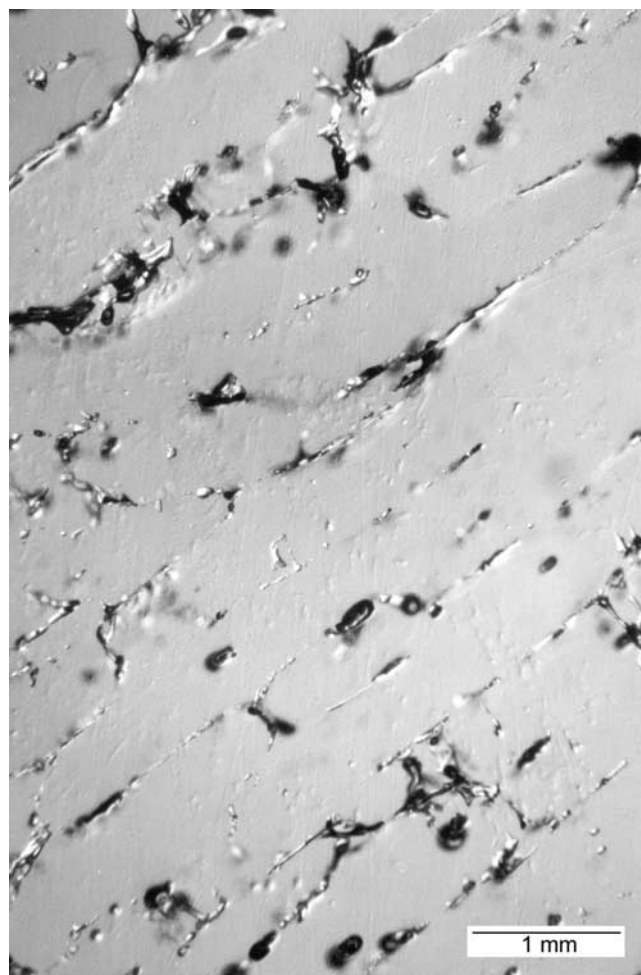


Figure 8. Horizontal micrographs obtained from a low-porosity band located between 1.045 and 1.08 m in the Chukchi Sea, April 2001.

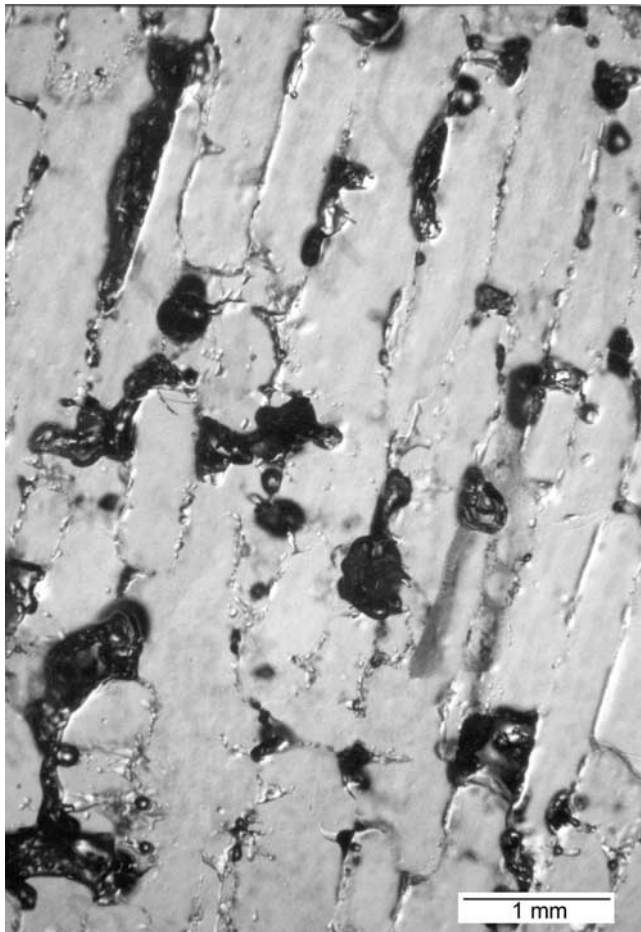


Figure 9. Horizontal micrograph obtained from a high-porosity band located between 1.255 and 1.265 in the Chukchi Sea, April 2001.

side of Figure 11 shows that the band consists of a population of large brine inclusions that generally nucleated and terminated at very well defined levels in the ice. Vertically oriented drainage networks have been observed to originate in these high-porosity bands and persist through subsequent low-porosity bands.

[27] Although the larger inclusions are generally oriented with their longest axis in the vertical direction, the micrographs show that they are frequently connected by a network of small lateral tubes, and *Cole et al.* [2002] present additional micrographs and inclusion size statistics on these features. In vertical sections oriented with the viewing direction coincident with the *c*-axis direction (e.g., the subgrain plates are viewed face on), the lateral brine tubes constitute an area fraction of 0.022 in a typical low-porosity band and 0.064 in an adjacent high-porosity band. These area fractions correspond to bulk band salinities of 2.3 and 6.5‰ for an in situ temperature of -5°C (estimated based on typical temperature gradients due to lack of in situ temperature data in the early ice season). Interestingly, these area fractions of brine inclusions are in approximately the same proportion as observed in the horizontal sections through low- and high-porosity bands noted above. The average diameters of the lateral tubes (calculated as the

diameter of a circle with an area equal to the object area determined by the image processor) ranged from 0.14 to 0.24 mm, with a tendency for larger-diameter tubes to form in the high-porosity bands. These observations suggest that there is sufficient connectivity to support lateral brine migration and hence preferential drainage of brine from the high-porosity bands. Additionally, we have observed these lateral tubes in the skeletal band, indicating that they form during initial freeze-up. Our observations of lateral brine tubes apply primarily to newly formed ice, or ice that has not warmed to the extent that extensive secondary brine drainage features have developed.

6.4. Very Low-Porosity Bands

[28] We occasionally observe thin bands with an exceptionally low level of brine porosity. They are laterally extensive, typically measure only several millimeters in the growth direction, and are frequently followed immediately by a high-porosity band. Figure 12 shows an example of such a band at three levels of magnification. These bands appear to be of the type described by *Gow et al.* [1987a, 1987b] in that they are very thin and much more optically clear than the adjacent ice containing a more usual array of brine inclusions. Since brine tubes frequently terminate at these bands, they could inhibit the downward flux of brine when the sheet begins to warm. An examination of the records indicates that at approximately the time of formation of this very low porosity band, the water temperature increased from an average value of 271.66 K to 272.11 K and then returned to the average value over a period of 1.2 days. It is interesting to note that this band coincides with the maximum values in $\delta^{18}\text{O}$ observed in the entire core (Figure 2a). This suggests possible advection of warmer water, possibly of deeper halocline/Atlantic origin, encroaching onto the shelf [*Cooper et al.*, 1997]. All other sources of warmer water capable of reduction in growth and melting would be associated with lower $\delta^{18}\text{O}$ as they would have to originate from a potential reservoir of warmer terrestrial runoff (including potential artifacts due to sewage lagoon discharge). From sea ice and water temperature (*H. Eicken and C. George*, unpublished data, 2003), it appears that such winter warming and melt events occurred several times in mid-winter during recent years. However, it is not clear at this point to what extent this is a local- or regional-scale phenomenon.

6.5. Brine Migration From High-Porosity Bands

[29] As noted above, the relatively high salinity of the high-porosity bands promotes the downward migration of brine in a process that has been referred to as brine corrosion [*Bennington*, 1967]. The origin of these features is immediately evident when they are viewed under cross-polarized light: The recrystallization and microscopic slush ice formation [see also *Light et al.*, 2003] that occurs during the course of brine migration produces a region of very fine-grained ice. Figure 13 shows a portion of a full-depth section and a corresponding micrograph to illustrate this type of feature.

6.6. Small-Scale Porosity Variations

[30] In 2000, we produced serial section sequences for the lower bands of Chukchi Sea ice using methods described by *Freitag* [1999] and *Eicken et al.* [2000]. Briefly, sea-ice

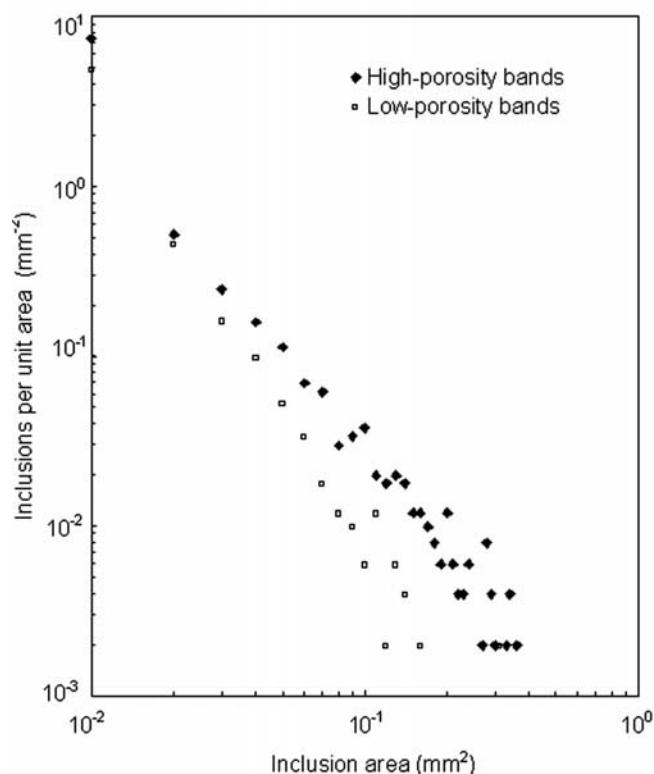


Figure 10. Inclusions per unit area versus cross-sectional area (in the horizontal plane) of brine tubes observed in the high- and low-porosity bands depicted in Figures 8 and 9. Note that the area density of small inclusions is approximately the same for both cases, but that the high-porosity bands have a higher population of larger-diameter inclusions.

cores, from which >90% of the resident brine has been removed through centrifuging as in situ temperatures, were cut into segments of several centimeters thickness, impregnated with an emulsion of titanium dioxide and oil and then microtomed. This results in a smooth ice surface, with all pores being filled by the white contrast agent. This surface was then recorded with a digital camera in obliquely incident light, and the process was repeated after removing fixed slices from the ice surface (on the order of 0.2 mm). The resulting section photographs were collocated with the help of reference points and through application of a cross-correlation technique to account for small-scale offsets between images. The resulting images were then stacked into a three-dimensional (3-D) array, and an automated segmentation algorithm was employed to distinguish between highly reflecting pores (due to the white titanium dioxide filling) and dark ice. The pixel size is approximately 60 μm , but with the preprocessing of images for the serial stacking, the minimum size pore size that can be identified is on the order of 100 μm . The porosity determinations take into account sub-pixel sized inclusions (each pixel is evaluated based on its mean gray value), so we can detect pores down to about 50 μm .

[31] The results in Figure 14 show that the porosity profiles have submillimeter resolution, and reflect the variations in pore structure associated with bands at depth. These data are from a core that was taken approximately 30 m away

from the location of the full-depth sections, approximately 1 week before the section in Figure 2e was obtained. A correspondence is evident between the porosity peaks in Figure 14 and the high-porosity bands near the bottom of Figure 2e. The indicated depths are somewhat out of registry as a result of thickness variations in the ice sheet (caused by snow cover variations).

[32] On the basis of field and laboratory measurements of porosity-permeability relationships [Freitag, 1999; Eicken *et al.*, 2004] the variations in porosity are associated with substantial permeability variations. The latter may be important in preconditioning an episodic discharge of brine from the skeletal band (as observed in single events by Wettlaufer *et al.* [1997]).

[33] The serial sections demonstrate that the local maxima and minima in porosity profiles can vary by as much as a factor of 2 over less than a centimeter depth interval. Clearly, routine field methods that typically determine salinity for 0.1-m-long core segments cannot resolve such fine-scale variations. Furthermore, the profile from the lowermost core section shows that the origins of these porosity variations lie in processes occurring within or just above the skeletal band.

7. Analysis of Horizontal Banding Features

[34] The full-depth sections seen in Figures 2a–2l provide a means to establish the spatial distribution of the bands. Additionally, for the years that ice growth was monitored at the field sites, we can calculate the time of formation of each band and thus gain insight into the periodicity of the underlying physical process. We monitored ice growth for the winters of 2000–2001 and 2001–2002, and data were obtained for the 2002–2003 season through another program (“Collaborative Research on

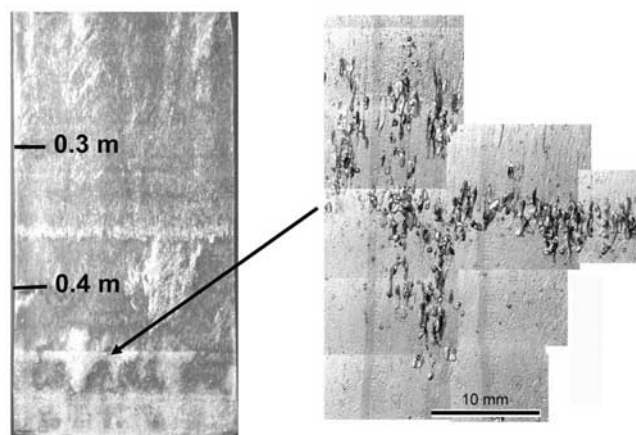


Figure 11. (left) Full-depth section of the ice sheet in the Chukchi Sea in December 2000 and (right) a composite micrograph of the high-porosity band observed at a depth of 0.45 m in the Chukchi Sea. Because of the lighting methods, the high-porosity bands in the full-depth section appear as light regions, and the large, drained brine inclusions in the composite micrograph appear as dark objects. Note the well-defined onset and termination of the larger inclusions that characterize this band. The finest gradations on the scales in the micrograph are 0.1 mm.

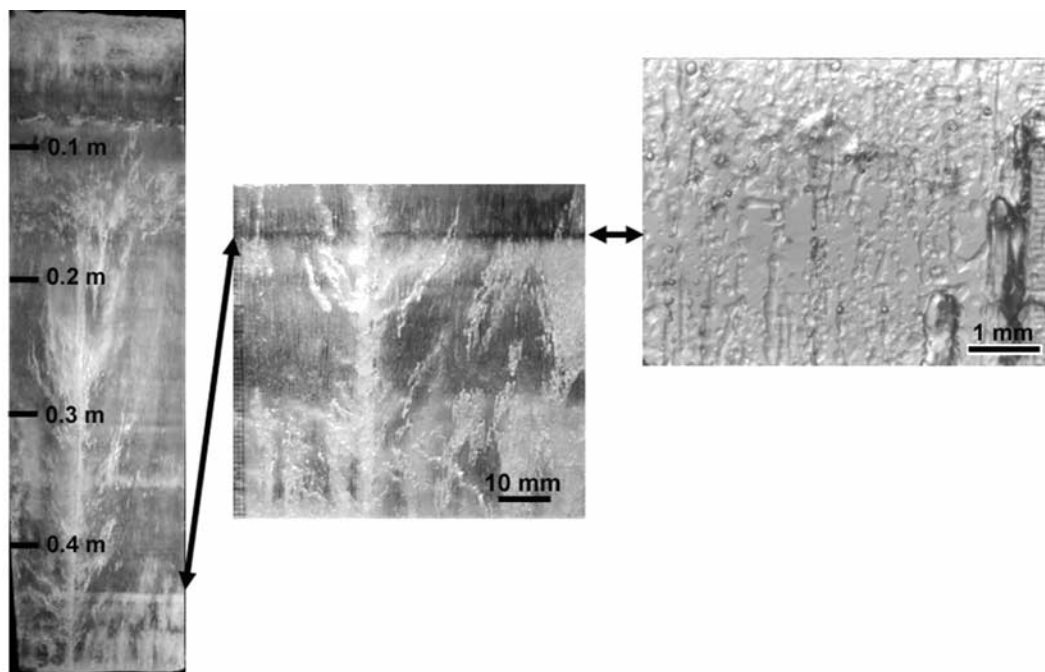


Figure 12. Sequence of vertical sections with increasing magnification showing a type of narrow, very low-porosity band that is occasionally observed. (Chukchi Sea, December 1999).

Long-Term Observations of the Energy and Mass Balance of Coastal Ice Covers in Northern Alaska” (OPP 9910300)).

[35] We employed a quantitative image processor (Image Pro Plus) to generate brightness profiles (corresponding to the gray value of pixels; e.g., Figure 2c) as a function of depth for the full-depth section images. Brightness values were averaged over regions ranging from approximately 0.1 to 0.3 m wide. The locations of these regions were selected to avoid vertical brine drainage features. Most of the digital

images were obtained by scanning 35-mm prints of the full-thickness sections (which measure $100\text{ mm} \times 150\text{ mm}$) at a resolution of 12 pixels mm^{-1} . The physical size of a pixel in the analyzed image ranged from 0.25 to 1 mm, depending on the area of the scanned photograph. Images for the sections in Figures 2h, 2i, and 2l were obtained with a digital camera that produced a resolution of approximately 1 mm per pixel.

[36] As a consequence of snow cover variations, the ice thickness where the full-depth sections were obtained was

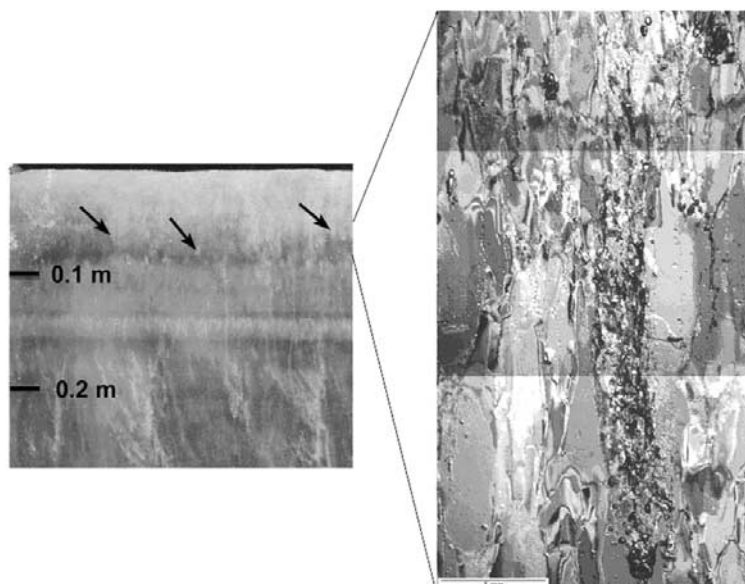


Figure 13. Example of brine corrosion associated with the high-porosity region near the top of the ice sheet (Chukchi Sea, April, 2000). (left) Banding in the upper portion of the ice sheet. The arrows indicate the location of several brine corrosion features. (right) Micrograph of a typical brine corrosion feature, from the indicated level in the sheet. See color version of this figure in the HTML.

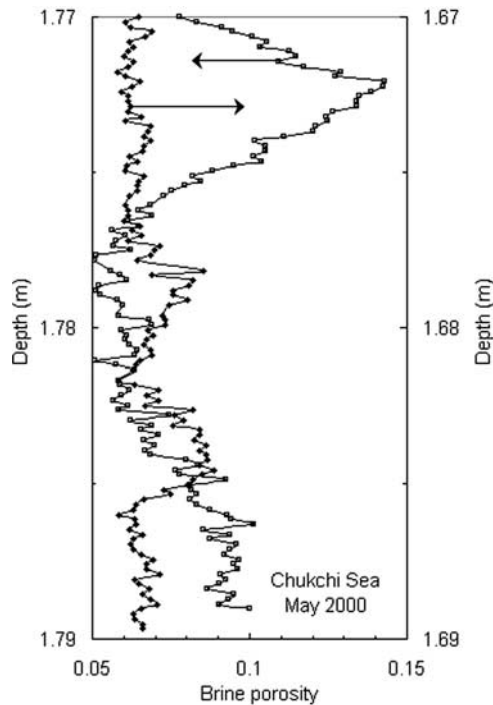


Figure 14. Examples of microscale brine porosity profiles generated by serial sectioning of cores from the lower bands of the Chukchi Sea ice sheet. The curves correspond to two segments of a core obtained just prior to the extraction of the full-depth section shown in Figure 2e, and the arrows indicate the respective depth scale. Note that the high-porosity bands evident in the porosity profile correspond to banding features in the bottommost section of the slab shown in Figure 2e.

occasionally different from that at the instrumented sites (typically some 30 m away, but on the same floe). For example, the full-depth sections were 0.2 m thicker than at the ice at the instrumentation site (1.70 versus 1.50 m) for the April 2001 observations (designated B9). To account for this, we scaled the ice thickness versus time relationship obtained at the instrumentation site to produce a thickness of 1.70 m (see Figure 15) for the date the full-depth sections were obtained. It is noted that the above scaling calculation implicitly assumes that the growth rate was uniformly higher during the entire growth period where the full-depth sections were obtained. That may not have been the case if the snow cover history where the full-depth sections were obtained differed from that of the instrumentation site.

[37] To analyze the bands as objectively as possible, their locations were determined from the brightness profiles using a numerical peak locator utility (provided in the commercial software package Dadisp). The resulting locations were visually compared with the full-depth section images, and a small number of peaks that did not correspond to visible features were eliminated. The total number and spacing of successive high-porosity bands thus identified, along with the associated statistics, are given in Table 1 for the indicated years. For the Chukchi Sea site, the number of bands ranged from 16 to 62, with a mean spacing of 0.054 to 0.024 m, respectively. As seen in Figure 16a, the analysis confirmed the visual observation that band spacing

did not vary systematically with depth. The number of bands found in the somewhat more limited data set for Elson Lagoon ranged from 23 to 51, with a mean spacing of 0.052 and 0.028 m, respectively. Figures 16b and 16c plot the frequency distribution of band spacing for the Chukchi Sea and Elson Lagoon sites, respectively.

[38] To calculate the time of formation of each band, and subsequently the time intervals between successive bands, we first conducted a polynomial best-fit analysis of the time versus thickness data. In most cases, the time-thickness data were analyzed in segments based on changes in curvature, allowing the use of relatively low-order polynomials to faithfully represent the data. The average time between the formation of successive bands and the related statistics from this analysis are reported in Table 1. Figures 16d and 16e plot the frequency distributions of the intervals between band formation for the indicated test sites and years. Interestingly, although the standard deviations are somewhat large, the average times between band formation for the three seasons of 1999–2002 were 3.2 ± 1.7 , 3.5 ± 1.9 , and 4.4 ± 3.6 days.

8. Discussion

[39] It is evident from a comparison of the full-depth sections in Figures 2a–2l that the banding characteristics (e.g., width and spacing of high-porosity bands) at a given site vary significantly from year to year. Furthermore, for a given year, the banding characteristics in the Chukchi Sea and in Elson Lagoon are not similar to each other. Since the two sites are only several kilometers apart and subject to approximately the same thermal history, it seems unlikely that the bands occurring at depth are caused by thermal fluctuations. Additionally, the observation that the average time between high-porosity bands is not a function of depth

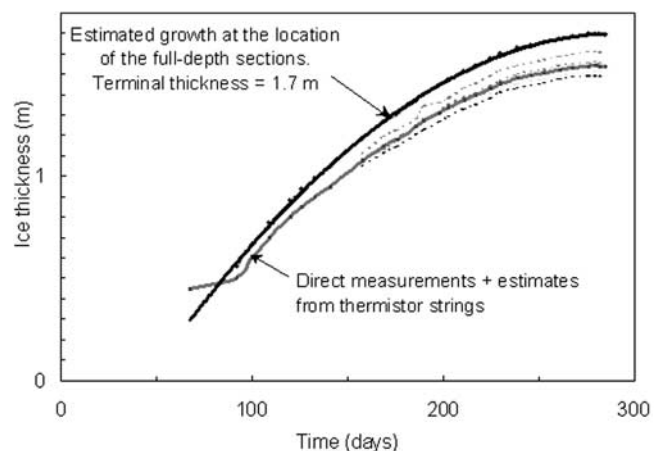


Figure 15. Thickness versus time for the Chukchi Sea test site. Direct measurements of ice thickness were combined with values inferred from temperature profiles to produce an average growth rate for each site. This average was then scaled to produce the maximum thickness (e.g., 1.7 m for the Chukchi Sea 2000–2001 growth season) observed at the location at which the full-depth sections seen in Figures 2a–2l were obtained. Data from four thermistor strings (shown in broken lines) were averaged to produce the lower curve.

Table 1. Summary of Banding Analysis Results

Full-Depth Section Identification	Date	Ice Thickness, m	Number of Bands	Mean Spacing, m	Standard Deviation, m	Time Between Bands, days	Standard Deviation, days	Frequency, day ⁻¹
B4-CSA2A	May 1995	1.34	44	0.029	0.012			
B5-CSA1	May 1999	1.25	16	0.054	0.034			
B8-CSA1	May 2000	1.70	54	0.030	0.020	4.41	3.56	0.23
B9-CSA2 (0.5 to 1.4 m)	April 2001	1.40	51	0.016	0.011			
B10-CSA1	May 2001	1.54	62	0.024	0.012	3.18	1.67	0.31
B10-ELA1	May 2001	1.45	51	0.028	0.016	3.69	2.31	0.27
B11-CSA1	May 2002	1.42	23	0.030	0.016	3.53	1.87	0.28
B11-ELA1	May 2002	1.20	23	0.052	0.040	7.48	5.57	0.13
B11-ELB1 (0.5–1.2 m)	May 2002	1.20	30	0.021	0.015	3.27	2.17	0.31

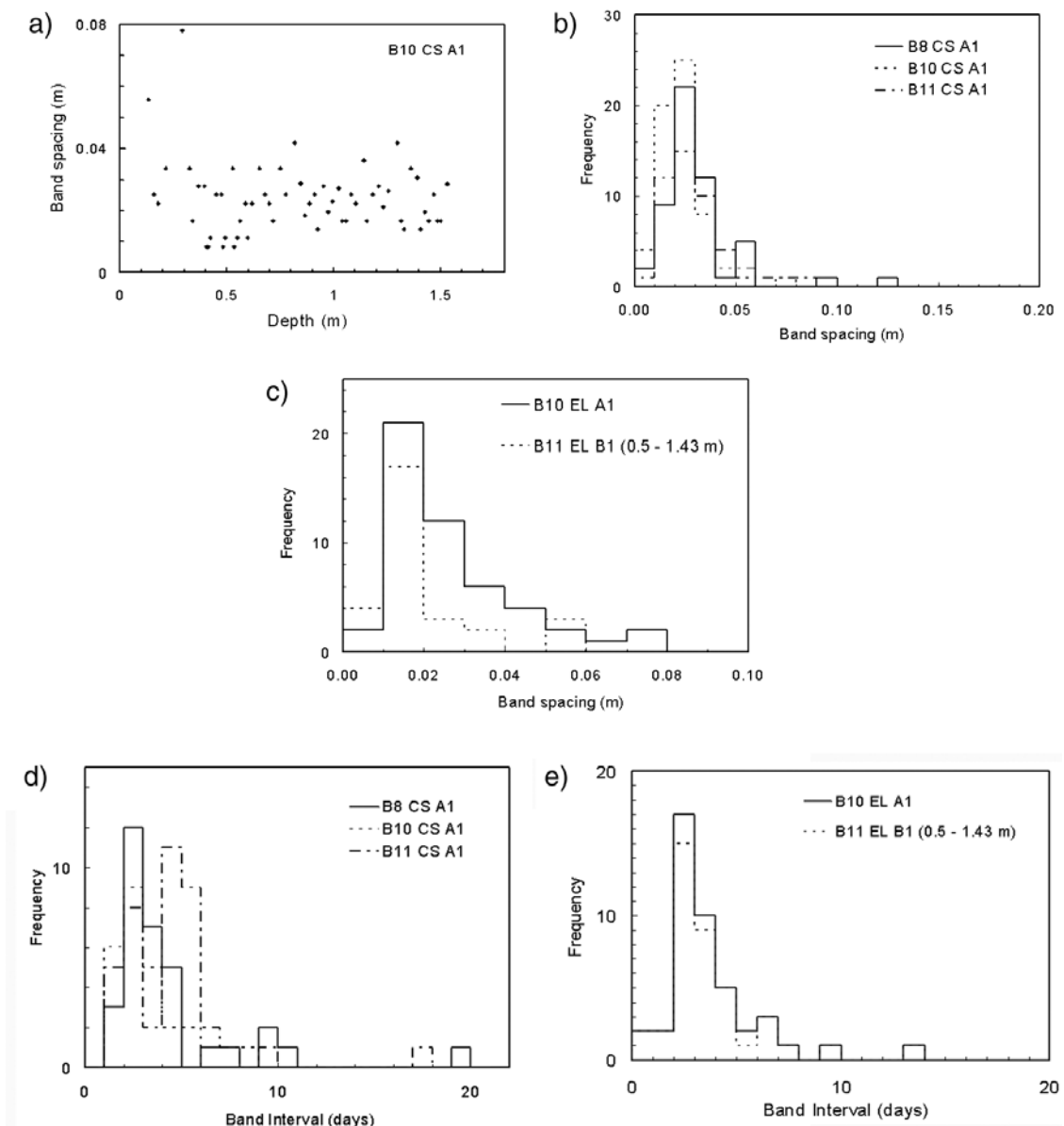


Figure 16. Spatial and temporal variations of bands in the Chukchi Sea and Elson Lagoon. (a) Band spacing versus depth in sheet for the Chukchi Sea site, April 2001. Frequency distributions of band spacing for (b) the Chukchi Sea and (c) Elson Lagoon. Frequency distributions of the time between the formation of adjacent bands in (d) the Chukchi Sea and (e) Elson Lagoon.

in the sheet argues against a process driven by thermal fluctuations at the ice surface and the resulting growth rate variations. The observation that the average time between the formation of successive bands is reasonably consistent (e.g., between 3.2 and 4.4 days) for several recent years provides a useful point of comparison with candidate processes. Specifically, as will be demonstrated in a subsequent publication, these values are in reasonably good agreement with the periodicity found in the local sea level fluctuations. The above considerations provide some support for a linkage between under-ice processes and band formation. Alternatively, the frequency distributions of band spacing with a consistent single maximum may possibly be an indication of an oscillatory brine discharge process [see *Niedrauer and Martin, 1979*].

[40] The observation that new crystals start growing in high-porosity bands but do not propagate beyond the band further suggests that the formation of high-porosity bands is related to a decrease in the velocity of the under-ice current. The newly nucleated crystals evident in Figure 6c are visible because their orientation is different from the highly aligned ice in which they are growing. One interpretation of this finding is that the velocity of the under-ice current dropped below the level needed to influence the alignment of the growing ice. Thus, since there is no growth preference for grains with a specific *c*-axis alignment, the unaligned grains were free to propagate. The reduced current also results in the growth of ice with higher brine porosity [Adams *et al.*, 1963; Eicken *et al.*, 2000]. A subsequent increase in the current reestablishes the growth preference for grains with their *c*-axes aligned with the current (e.g., grains that are not aligned with the current are grown out of existence) and causes a decrease in the brine porosity of the newly forming ice.

[41] As noted above, brine inclusions with widths that are approximately equal to the plate spacing are common in the high-porosity bands and in fact account for nearly half of the total area fraction of brine inclusions in these bands. By contrast, ~11% of the horizontal area fraction of brine inclusions in a typical low-porosity band are associated with inclusions having widths >0.5 mm. Given these observations, it may be useful to develop separate distributions for the small inclusions that persist through most of the banding features, and the large inclusions that form primarily in the high-porosity bands. On a fundamental level, it would be especially useful to determine the precise conditions of growth that trigger the formation of these larger-diameter inclusions.

[42] With regard to the lateral tubes that connect adjacent plate boundaries, we note that although these tubes are substantially larger and more populous in the high-porosity bands, they are nonetheless present in the low-porosity bands. The area fraction of these tubes, as measured in vertical sections through either low- or high-porosity bands, is approximately two thirds of the associated horizontal area fraction. The lateral tubes can presumably support the horizontal movement of brine generally throughout the sheet, but given our observations noted above, later brine movement occurs most readily in the high-porosity bands.

[43] The observations in the preceding paragraph shed light on a question raised in regard to deformation-drive brine drainage. *Perovich et al.* [1995] studied ice stalactites in

the Alaskan Beaufort Sea and found that they grew under deforming lead ice as a result of extensive brine drainage. Sections of the ice were tilted as a consequence of rafting, and this promoted gravity drainage of brine toward low points. The stalactites formed at the points where the cold brine exited the sheet. However, the question of what drainage features in the young ice would support the lateral movement of the necessary amount of brine remained open. Our results suggest that the horizontal movement of brine could be readily supported by the population of lateral brine tubes that naturally form in high-porosity bands in the lead ice.

9. Summary and Conclusions

[44] Full-depth sections of the land-fast, first-year sea ice in the Chukchi Sea near Barrow, Alaska, and in Elson Lagoon exhibit pronounced horizontal banding features. These features have been examined on the scale of meters to the scale of the constituent brine inclusions (10^{-4} m). Images of full-depth sections from several seasons at both study sites illustrated a variety of high- and low-porosity bands. We examined a number of representative bands using photomicroscopy and image analysis techniques to quantify the size distribution and area density of the brine inclusions. This analysis indicated that the total area of inclusions for the high-porosity bands, when viewed in a horizontal cross section, was nearly 3 times that of the low-porosity bands. Ice growth records were employed to establish the time of formation of the bands, and this analysis revealed a reasonably consistent average time between the formation of successive bands for three study years. Crystallographic aspects of various banding features were examined as well.

[45] From the observations and analysis presented above, we concluded the following:

[46] 1. Horizontal banding can occur generally throughout the entire depth of first-year sea ice sheets, and neither the thickness of the bands nor their spacing appears to correlate with depth.

[47] 2. As measured on horizontal sections, the area fraction of brine inclusions in the high- and low-porosity bands was 0.091 and 0.034, respectively.

[48] 3. The microscopy showed that there is a significant degree of interconnectedness in the horizontal plane among the brine inclusions in high-porosity bands. This is believed to explain the observed tendency of such bands to drain preferentially. However, this may not be the case for warm ice that has experienced a significant amount of brine drainage.

[49] 4. In addition to a population of small brine inclusions that are consistent with observations in the low-porosity bands, the high-porosity bands contain a population of large brine tubes with diameters that are approximately equal to the plate spacing.

[50] 5. In the years for which growth rate data were available, calculations indicated that the average times between the formation of successive high-porosity bands were 3.2 ± 1.7 , 3.5 ± 1.9 and 4.4 ± 3.6 days.

[51] **Acknowledgments.** This work was funded under the Arctic Natural Sciences Program of the National Science Foundation's Office of Polar Programs (projects OPP-9813221 and OPP-9872573), and we are grateful for the support of program managers Jane Dionne and Neil

Swanberg of that organization. We gratefully acknowledge the expert and diligent assistance of David Ramey and other personnel from the Barrow Arctic Science Consortium of Barrow, Alaska, during the execution of the many field trips associated with this project. We also acknowledge support from the Office of Naval Research's Sea Ice Mechanics Initiative, under which the full-depth sections from 1994 and 1995 were obtained. Johannes Freitag, Sven Grage, and Andy Mahoney provided help in the field and the lab. Stable-isotope measurements were kindly provided by Gordon Bower and Nori Tanaka (Frontier Research Program, International Arctic Research Center). Emily Andreas conducted the inclusion size analysis. A CD entitled "Inside Sea Ice-I" is available from the lead author. It contains details on the field observations that were conducted under this program, photographs of the full-depth sections, and sets of orthogonal thin section photographs and high-resolution micrographs obtained at 0.1-m intervals through the ice sheet at our Chukchi Sea test site.

References

- Adams, C. M., Jr., D. N. French, and W. D. Kingery (1963), Field solidification and desalination of sea ice, in *Ice and Snow: Properties, Processes and Applications*, edited by W. D. Kingery, pp. 277–288, MIT Press, Cambridge Mass.
- Bennington, K. O. (1963a), Some chemical composition studies on Arctic sea ice, in *Ice and Snow: Properties, Processes and Applications*, edited by W. D. Kingery, pp. 248–257, MIT Press, Cambridge Mass.
- Bennington, K. O. (1963b), Some crystal growth features of sea ice, *J. Glaciol.*, *4*, 669–688.
- Bennington, K. O. (1967), Desalination features in natural sea ice, *J. Glaciol.*, *6*, 845–857.
- Cole, D. M., and J. P. Dempsey (2004), In-situ sea ice experiments in McMurdo Sound: Cyclic loading, fracture and acoustic emissions, *J. Cold Reg. Eng.*, in press.
- Cole, D. M., and G. D. Durell (2001), A dislocation-based analysis of strain history effects in ice, *Philos. Mag. A.*, *81*, 1849–1872.
- Cole, D. M., and L. H. Shapiro (1998), Observations of brine drainage networks and microstructure of first-year sea ice, *J. Geophys. Res.*, *103*(C10), 21,739–21,750.
- Cole, D. M., L. H. Shapiro, W. F. Weeks, C. Byers, J. P. Dempsey, R. M. Adamson, V. F. Petrenko, and O. V. Gluschenkov (1995), Overview of a recent program on the mechanical properties of sea ice, *J. Cold Reg. Eng.*, *9*, 219–234.
- Cole, D. M., H. Eicken, K. Frey, and L. H. Shapiro (2002), Some observations of high porosity bands and brine drainage features in first-year sea ice, paper presented at 16th International Ice Symposium, Int. Assoc. for Hydraul. Res., Dunedin, New Zealand.
- Cooper, L. W., T. E. Whitledge, J. M. Grebmeier, and T. Weingartner (1997), The nutrient, salinity, and stable oxygen isotope composition of Bering and Chukchi Seas waters in and near the Bering Strait, *J. Geophys. Res.*, *102*(C6), 12,563–12,573.
- Cox, G. F. N., and W. F. Weeks (1983), Equations for determining the gas and brine volumes in sea-ice samples, *J. Glaciol.*, *29*(102), 306–316.
- Eicken, H., C. Bock, R. Wittig, H. Miller, and H.-O. Poertner (2000), Nuclear magnetic resonance imaging of sea ice pore fluids: Methods and thermal evolution of pore microstructure, *Cold Reg. Sci. Technol.*, *31*, 207–225.
- Eicken, H., T. C. Grenfell, D. K. Perovich, J. A. Richter-Menge, and K. Frey (2004), Hydraulic controls of summer Arctic pack ice albedo, *J. Geophys. Res.*, *109*, C08007, doi:10.1029/2003JC001989.
- Freitag, J. (1999), The hydraulic properties of Arctic sea ice—Implications for the small-scale particle transport (in German), *Ber. Polarforsch.*, *325*, 150 pp.
- Frey, K., H. Eicken, D. K. Perovich, T. C. Grenfell, B. Light, L. H. Shapiro, and A. P. Stierle (2001), Heat budget and decay of clean and sediment-laden sea ice off the northern coast of Alaska, paper presented at Port and Ocean Engineering in the Arctic Conference (POAC'1), Secr., Norw. Hydrotech. Lab., Trondheim, Norway.
- Gow, A. J., W. B. Tucker, and W. B. Weeks (1987a), Physical properties of summer sea ice in the Fram Strait, June–July 1984, *Rep. 87-16*, Cold Reg. Res. and Eng. Lab., Hanover, N. H.
- Gow, A. J., S. F. Ackley, K. R. Buck, and K. Golden (1987b), Physical and structural characteristics of Weddell Sea pack ice, *Rep. 87-14*, Cold Reg. Res. and Eng. Lab., Hanover, N. H.
- Light, B., G. A. Maykut, and T. C. Grenfell (2003), Effects of temperature on the microstructure of first-year sea ice, *J. Geophys. Res.*, *108*(C2), 3051, doi:10.1029/2001JC000887.
- Niedrauer, T. M., and S. Martin (1979), An experimental study of brine drainage and convection in young sea ice, *J. Geophys. Res.*, *84*(C3), 1176–1186.
- Perovich, D. K., and A. J. Gow (1991), A statistical description of the microstructure of young sea ice, *J. Geophys. Res.*, *96*(C9), 16,943–16,953.
- Perovich, D. K., and A. J. Gow (1996), A quantitative description of sea ice inclusions, *J. Geophys. Res.*, *101*(C8), 18,327–18,343.
- Perovich, D. K., J. A. Richter-Menge, and J. H. Morison (1995), The formation and morphology of ice stalactites observed under deforming lead ice, *J. Glaciol.*, *41*(138), 305–312.
- Perovich, D. K., C. Roesler, and W. S. Pegau (1998), Variability in Arctic sea ice optical properties, *J. Geophys. Res.*, *103*(C1), 1193–1208.
- Perovich, D. K., et al. (2001), Arctic Coastal Processes Data Report 2001 [CD-ROM], Cold Reg. Res. and Eng. Lab., Hanover, N. H.
- Phelps, A. R., and M. O. Jeffries (1999), Inclusion of methane in bubbles in ice on shallow, high latitude lakes, in *Ice Physics and the Natural Environment*, edited by J. Wettlaufer, J. G. Dash, and N. Untersteiner, pp. 335–339, Springer-Verlag, New York.
- Phelps, A. R., K. Peterson, and M. O. Jeffries (1998), Methane efflux from high-latitude lakes during spring ice-melt, *J. Geophys. Res.*, *103*(D2), 29,029–29,036.
- Schwerdtfeger, P. (1963), The thermal properties of sea ice, *J. Glaciol.*, *4*, 789–807.
- Smith, I. J., P. J. Langhorne, H. J. Trodahl, T. G. Haskell, and D. M. Cole (1998), Platelet ice—The McMurdo Sound debate, paper presented at 14th International Symposium on Ice, Int. Assoc. for Hydraul. Res., Potsdam, N. Y.
- Stierle, A. P., and H. Eicken (2002), Sedimentary inclusions in Alaskan coastal sea ice: Small-scale distribution, interannual variability and entrainment requirements, *Arct. Antarct. Alp. Res.*, *34*, 103–114.
- Verbeke, V., J.-L. Tison, H.-J. Trodahl, and T. G. Haskell (2002), Banding in McMurdo Sound fast ice, paper presented at 16th International Ice Symposium, Int. Assoc. for Hydraul. Res., Dunedin, New Zealand.
- Weeks, W. F., and S. F. Ackley (1982), The growth, structure, and properties of sea ice, *Monogr. 82-1*, 130 pp., Cold Reg. Res. and Eng. Lab., Hanover, N. H.
- Weeks, W. F., and A. J. Gow (1978), Preferred crystal orientations in the fast ice along the margins of the Arctic Ocean, *J. Geophys. Res.*, *83*(C10), 5105–5121.
- Wettlaufer, J. S., M. G. Worster, and H. E. Huppert (1997), The phase evolution of young sea ice, *Geophys. Res. Lett.*, *24*, 1251–1254.

D. M. Cole, U.S. Army Cold Regions Research and Engineering Laboratory, 72 Lyme Road, Hanover, NH 03755, USA. (david.m.cole@erdc.usace.army.mil)

H. Eicken and L. H. Shapiro, Geophysical Institute, University of Alaska Fairbanks, 903 Koyukuk Drive, P. O. Box 757320, Fairbanks, AK 99775-7320, USA. (hajo.eicken@gi.alaska.edu; lews@gi.alaska.edu)